coatings

MDPI

Article

MicroRaman Study of Nanostructured Ultra-Thin AlGaN/GaN Thin Films Grown on Hybrid Compliant SiC/Por-Si Substrates

Aleksandr Lenshin [1,2,*], Pavel Seredin [1,3], Dmitry Goloshchapov [1], Ali O. Radam [1] and Andrey Mizerov [4]

[1] Solid State Physics and Nanostructures Department, Voronezh State University, 394018 Voronezh, Russia; paul@phys.vsu.ru (P.S.); goloshchapov@phys.vsu.ru (D.G.); radam@phys.vsu.ru (A.O.R.)
[2] Physics Department, Voronezh State University of Engineering Technologies, Prospect of Revolution 19, 394000 Voronezh, Russia
[3] Scientific and Educational Center "Nanomaterials and Nanotechnologies", Ural Federal University Named after the First President of Russia B. N. Yeltsin, Mir av., 620002 Yekaterinburg, Russia
[4] Physics Department, St. Petersburg National Research Academic University of the Russian Academy of Sciences, 8 Khlopin St., Building 3, lit. A, St. 194021 Petersburg, Russia; mizerov@mail.ru
* Correspondence: lenshinas@mail.ru

Abstract: In our study, for the first time we demonstrate the advantages of using a compliant hybrid substrate of porSi/SiC to grow high-quality ultra-thin nanostructured $Al_xGa_{1-x}N$/GaN heterostructures using molecular beam epitaxy with plasma-activated nitrogen. Comparison of our experimental results obtained by micro-Raman spectroscopy, deconvolution, and the fitting of the experimental Raman spectra and subsequent calculations with information from already established literature sources show that the use of such a hybrid SiC/porSi substrate has a number of undeniable advantages for the growth of ultra-thin $Al_xGa_{1-x}N$/GaN nanoheterostructures without requiring the use of thick $A_{III}N$ buffer layers. Direct growth on a hybrid compliant substrate of SiC/porSi leads to a substantial relaxation in the elastic stresses between the epitaxial film, porous silicon, and silicon carbide, which consequently affects the structural quality of the ultra-thin $Al_xGa_{1-x}N$/GaN epitaxial layers. The experimental and computational data obtained in our work are important for understanding the physics and technology of $Al_xGa_{1-x}N$/GaN nanoheterostructures and will contribute to their potential applications in optoelectronics.

Keywords: porous silicon; $A_{III}N$; Raman spectroscopy

check for updates

Citation: Lenshin, A.; Seredin, P.; Goloshchapov, D.; Radam, A.O.; Mizerov, A. MicroRaman Study of Nanostructured Ultra-Thin AlGaN/GaN Thin Films Grown on Hybrid Compliant SiC/Por-Si Substrates. *Coatings* **2022**, *12*, 626. https://doi.org/10.3390/coatings12050626

Academic Editor: Choongik Kim

Received: 7 April 2022
Accepted: 29 April 2022
Published: 3 May 2022

1. Introduction

The semiconductor industry has undergone a paradigm shift, from scaling the physical size of a single device to using new and innovative materials. Examples of such materials include the Al-Ga-N semiconductor compounds of group-III nitrides, which offer a unique combination of piezoelectric, electrical, mechanical, chemical, and optical properties. At present, they are one of the most promising systems of semiconducting materials that are used to develop and create various sensors and transmitters of physical quantities, including those suitable for harsh environments (elevated temperatures, radiation, and aggressive media) [1]. They became a basis for the creation of effective nanoscale quantum devices operating in the microwave range (e.g., transistors with high electron mobility (HEMT), tunneling diodes, resonant tunneling diodes, or phototransistors) [2,3], in high-power and high-frequency applications [4], one- or two-dimensional (1D/2D) hybrid systems applied in high-performance self-powered photodetection [5], as well as light-emitting diodes (LED) and photodetectors operating in the ultraviolet range of the spectrum.

The active development of epitaxial growth approaches for $A_{III}N$-stressed heterostructures enables the design and fabrication of optoelectronic devices, covering a very wide range of applications. However, ever-increasing demands on the performance of designed optoelectronic devices, lower power consumption, and, consequently, higher efficiency

with, most importantly, lower manufacturing costs, require the integration of optical functional elements of $A_{III}N$ with a silicon substrate. However, the development of $A_{III}N$ metal-oxide-semiconductor (CMOS) structures has proved challenging because of the lack of a suitable strategy for $A_{III}N$ integrating on a Si single substrate. The non-centrosymmetric wurtzite structure and appreciable electronegativity differences between nitrogen and group-III elements induce strong polarization effects in III–nitride compounds [6]. At the same time, significant differences between lattice constants and the thermal expansion coefficients of nitride $A_{III}N$ compounds and silicon compounds make it very difficult to grow high-quality crystal instrumental heterostructures. Thus, the creation of structurally perfect $A_{III}N$/Si requires a growth technology that can provide effective relaxation of the residual stresses of the heteropair crystal lattice mismatch, as well as the filtration of dislocations sprouting into the active region of the device heterostructure.

In recent years, buffer layers of nitrides [7,8], multi-period superlattices, layers with an alternating 2D and 3D morphology, layers with a composition gradient, etc., as well as combinations of these structures have mainly been used to solve this problem. Recently, there has been great interest in the use of more lattice-consistent SiC/Si hybrid substrates for the epitaxy of $A_{III}N$ heterostructures [9–11]. In addition, as has been repeatedly demonstrated, one of the more promising approaches to the growth of hybrid $A_{III}N$/Si structures is the use of nanoporous silicon layers (porSi) or nanoprofiled silicon substrate surfaces (protoSi) [12–15]. Epitaxial $A_{III}B_V$ compound semiconductor layers, grown by metal–organic chemical vapor deposition (MOCVD) or molecular beam epitaxy with plasma-activated nitrogen (PAMBE) using this approach, had better structural quality as well as optical properties compared to their counterparts that were grown under similar conditions on crystalline silicon, cSi. Prior research has shown that the introduction of a 3C-SiC layer created by the Kukushkin method [16] on a substrate with a previously formed nanoporous silicon sublayer also has a number of undeniable advantages over standard substrates. It results in a more uniformly high-quality GaN layer without visible extended defects and allows for unique optical and electrophysical characteristics to be achieved in the GaN/SiC hybrid heteroepitaxial structures.

However, it should be noted that the promising approach of using more lattice-consistent SiC/porSi hybrid substrates for the epitaxy of $A_{III}N$ heterostructures has not been widely used so far, not least because of the lack of reproducible technology for producing defect-free silicon carbide layers on preformed porous silicon Si layers over a sufficiently large area at a reasonable cost. However, according to our data, there are no reports in the literature on the epitaxial synthesis of ultra-thin $Al_xGa_{1-x}N$/GaN nanostructures directly layered on substrates incorporating SiC and porSi layers without using thick $A_{III}N$ buffer layers.

The aim of this study was a demonstration of the advantages of using a compliant hybrid substrate containing porous silicon (porSi) and silicon carbide (SiC) layers to grow high-quality ultra-thin nanostructured $Al_xGa_{1-x}N$/GaN heterostructures by molecular beam epitaxy using plasma-activated nitrogen, with the help of micro-Raman spectroscopy results.

2. Materials and Methods

Heterostructures based on layers of the Al-Ga-N system were grown using plasma-assisted molecular beam epitaxy (PAMBE) on a Veeco Gen 200 multi-wafer MBE reactor (Plainview, NY, USA) [17]. A schematic representation of the developed structures is shown in Figure 1.

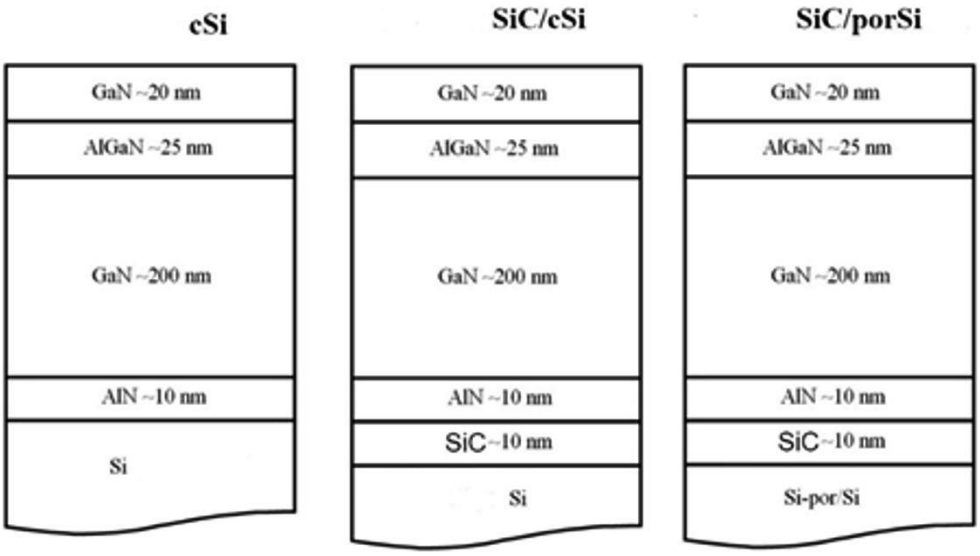

Figure 1. Design of the investigated heterostructures.

Two-inch boron-doped cSi crystalline silicon wafers with an orientation of (111) and resistivity of <10 Ω × cm^2 were used to grow heterostructures in a single PAMBE process. Three types of substrates were used: an initial crystalline silicon substrate, cSi, a silicon substrate on whose surface a silicon carbide layer, SiC/cSi, was formed using the Kukushkin method [18], and a silicon substrate with a porous sublayer and a silicon carbide layer obtained using the Kukushkin method—SiC/porSi.

Porous silicon samples were obtained by electrochemical etching. A solution of hydrofluoric acid and isopropyl alcohol was used as the etching solution, with an ECT current density of ~50 mA/cm^2. After obtaining the samples, they were washed in distillate to remove the residual reaction products [19].

Before the PAMBE synthesis of $Al_xGa_{1-x}N$/GaN nanoheterostructures, the cSi substrate was prepared according to the Shiraki method. The substrates with the SiC layer were degreased. Afterward, all three types of substrates were loaded into one substrate holder of the PAMBE unit and were then annealed in the pre-annealing chamber at 200 °C. Then, they underwent a final pre-epitaxial preparation in the growth chamber of the PAMBE unit at a temperature measured by a pyrometer at T = 850 °C for 30 min, in a flow of activated nitrogen, corresponding to an equivalent growth rate of GaN of the order of F_N~0.05 μm/h.

Afterward, to achieve the growth of $Al_xGa_{1-x}N$/GaN nanoheterostructures, the substrate temperature was reduced to T = 715 °C, i.e., to the temperature at which AlN decomposition in a vacuum is not observed and the decomposition rate of GaN (nitrogen desorption rate) becomes comparable to that of GaN, amounting, according to the authors of [20], to about $F_{des}{}^N$~0.01 μm/h.

The synthesis of $Al_xGa_{1-x}N$/GaN nanoheterostructures began with the formation of nucleated AlN layers of ~10 nm thickness on the substrate surfaces at $F_{Al} = F_N$~0.05 μm/h for 20 min. Then, a GaN layer was grown on the AlN surface at F_{Ga}~0.4 μm/h and F_N~0.05 μm/h for 5 h. Considering GaN decomposition, the actual growth rate of GaN, in this case, is $v^{GaN} = F_N - F_{des}{}^N$~0.04 μm/h. Thus, it was assumed that a GaN layer of ~200 nm thickness was grown.

After GaN growth, the in situ opening of the Al shutter was carried out, then $Al_xGa_{1-x}N$ layer growth was started at F_{Al}~0.02 μm/h, F_{Ga}~0.4 μm/h, and F_N~0.05 μm/h for 25 min. Once the $Al_xGa_{1-x}N$ layer had grown, the Al shutter was closed and an upper GaN layer with a thickness of ~20 nm was grown.

It should be noted that the fluxes of Ga, Al, and activated nitrogen, expressed in terms of the units of GaN and AlN growth rates, were determined in the preliminary calibration experiments as follows. First, using the Bayard-Alpert gauge, the values of the

beam equivalent pressures (BEP) of Ga and Al were measured at the different temperatures of these sources in a standard way. After that, preliminary growth experiments were carried out in which GaN or AlN layers were grown under nitrogen-rich conditions at substrate temperatures of T~650 and T~700 °C, respectively. Therefore, the growth run took place at temperatures at which the desorption rate of Ga and Al adatoms is much lower than the growth rate of GaN and AlN layers. The rough surface morphology of the growing layers provided by nitrogen-rich conditions was monitored in-situ by a spotty reflected high-energy electron diffraction pattern. In each single growth experiment, the fixed temperatures of the Ga or Al sources were used, while in the subsequent experiment, the temperature values of the Ga or Al sources were set differently from the previous one. The nitrogen flow was constant in all experiments. After the growth experiments, the thicknesses of the layers were measured using scanning electron microscope (SEM) in order to determine the growth rate of each layer. Thus, the relationship between the growth rates of GaN and AlN, and the BEP of Ga and Al atoms, respectively, were determined. In order to determine the flux of activated nitrogen, GaN and AlN layers were grown and examined using SEM under metal-rich growth conditions with two-dimensional surface morphology.

At the same time, in the experiments described in the work, the higher growth temperatures of T~715 °C were used. This resulted in an increase in nitrogen desorption from GaN (GaN decomposition rate) on the value of $F_{des}{}^{N}$~0.01 μm/h (according to Fernández-Garrido et al. [20]), which should be taken into account when calculating the thicknesses of the layers containing GaN, as well as when calculating the compositions of AlGaN solid solutions.

The reproducibility of layer thicknesses in heterostructures grown under the same conditions was evaluated using SEM measurements. In terms of the rather thin heterostructures that were grown, this technique did not show any significant differences in the thicknesses of the layers.

The samples were diagnosed using a set of structural spectroscopic methods of analysis.

Micro-Raman scattering spectra were obtained. All spectra were obtained in the range of 100–4000 cm^{-1}, using the confocal RamMix 532 Raman microscope (InSpectr, Moscow, Russia) with a spectral resolution of 1 cm^{-1}. Excitation was performed using a 532 nm wavelength laser with ~30 mW of radiation power at the sample. The choice of the microregions and the mapping on the surface of the samples were realized using an automated motorized 2-axis stage, providing minimum step-by-step shifts of 300 nm. A signal from the surface of a sample was collected with a 60× objective. The area of the analyzed microregion was 1 × 1 μm^2.

3. Results and Discussion

Based on the results of X-ray diffraction (XRD) (figures not presented in this work) we confirmed that the GaN and $Al_xGa_{1-x}N$ epitaxial layers included in the thin film nanoheterostructure have a wurtzite crystal structure. At the same time, the SiC layer formed by atomic substitution has the symmetry of a cubic 3C-SiC polytype, while the use of a nanoporous silicon porSi sublayer, obtained through electrochemical etching, hosted an oriented growth of silicon carbide.

The application of atomic force microscopy (AFM) in semicontact mode allowed the surface roughness of the heterostructures to be assessed, as well as the shape of the nanocolumns, depending on the type of substrate used. The average roughness values for the cSi, SiC/sSi, and SiC/porSi samples were 4.3, 6.6, and 10.9 nm, respectively. From the AFM data analysis, we determined the average lateral sizes of the nanocolumns to be ~70, ~91, and ~107 nm for the samples grown using cSi, SiC/cSi, and SiC/porSi substrates, respectively.

To obtain additional potentially useful and accurate information about the fine structural properties of the materials under study, we used Raman spectroscopy, which is based on the analysis of phonon spectra [21,22]. Since the lattice vibration spectra are very sensitive to the configuration of the nearby atoms, the use of Raman spectroscopy makes it

possible to study the features of the crystal structure of thin epitaxial layers and its imperfection rate on a scale of the order of magnitude of the crystal lattice parameters [13,23,24].

Figure 2 shows the Raman spectra for epitaxial heterostructures grown on three types of substrates.

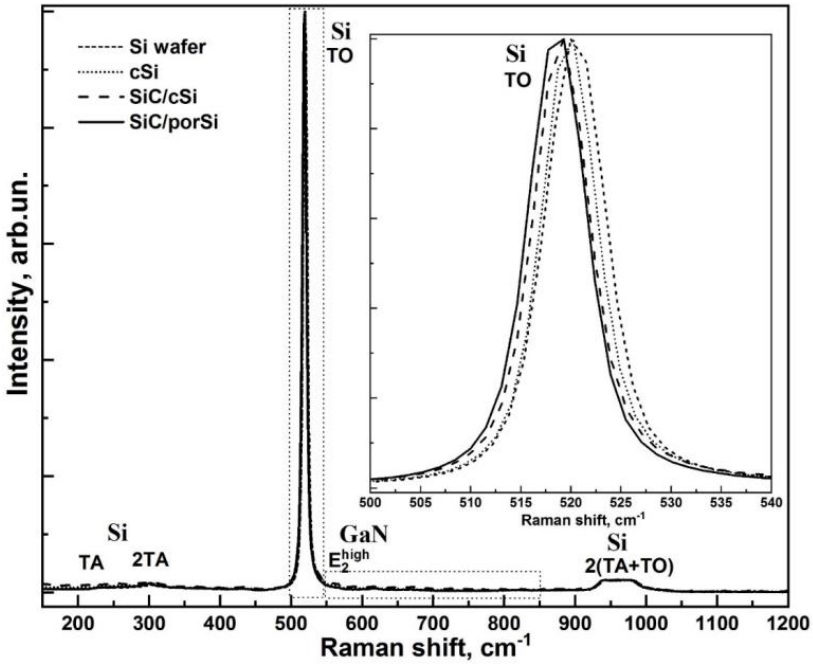

Figure 2. Raman spectra of epitaxial heterostructures grown on three types of substrates.

It follows from the data obtained that the most intense vibrational mode in the spectra of all heterostructures is the phonon mode, in the region of ~521 cm^{-1}, correlated with the transverse optical (TO) phonon of the silicon substrate at the central point of the Brillouin zone and characterized by a small width at half the peaks' height of FWHM (see Figure 2). The second and less intense order for this reflection (2TO Si) is in the region of ~1000 cm^{-1}. The analysis shows that in addition to the low-intensity oscillations of silicon, which are transverse acoustic phonons of the first (Si_{TA}~240 cm^{-1}) and second (Si_{2TA}~300 cm^{-1}) orders [25], longitudinal acoustic phonon-mode Si_{LA} (~300 cm^{-1}) [25] are active in heterostructural spectra. The oscillations located around 620 and 680 cm^{-1} are a combination of $Si_{TO\ (X)+TA\ (X)}$ and $Si_{TO\ (\Sigma)+TA}$ (Σ) phonons, respectively [26].

It should be noted that, as the inset to Figure 2 clearly shows, the TO mode of silicon experiences a characteristic low-frequency shift depending on the type of substrate used, relative to the TO mode position in the spectrum of the silicon wafer. It is clearly noticeable that this mode has the largest shift (~2 cm^{-1}) in the spectrum of the SiC/porSi sample, while in the spectra of cSi and SiC/cSi samples this shift is ~0.5 cm^{-1}. A significant shift (~2 cm^{-1}) of the silicon TO mode for SiC/porSi sample relative to its position for Si single crystal is due to the occurrence of deformations in the crystal lattice of the porous layer [27,28]; this is typical in the formation of a porous interlayer with a porosity value of ~40%, which correlates with the data reported by the authors of [29].

The relationship reported by the authors of [30] can be depicted thus:

$$\sigma_{xx} = \Delta\omega(232P - 190) \quad (1)$$

where σ_{xx} is the in-plane biaxial residual stress (MPa), and P is the porosity value of silicon (porosity is defined as the volume fraction of voids within the PS layer and can be determined easily via weight measurement). The residual stresses in the SiC/porSi substrate porous layer structure were estimated at 200 MPa for a given porosity value.

Figure 3 zooms in on the 530–900 cm^{-1} region of the experimental Raman spectra of the investigated heterostructures shown in Figure 2. In addition, Figure 2 shows the Raman spectrum of a single crystal silicon wafer used for the three types of wafers, as well as the reference spectrum of silicon carbide, obtained using the Kukushkin method. The spectra are presented without baseline correction or the removal of the silicon-wafer TO mode from the spectrum, which allows us to visualize the low-intensity vibrations in the Raman spectra.

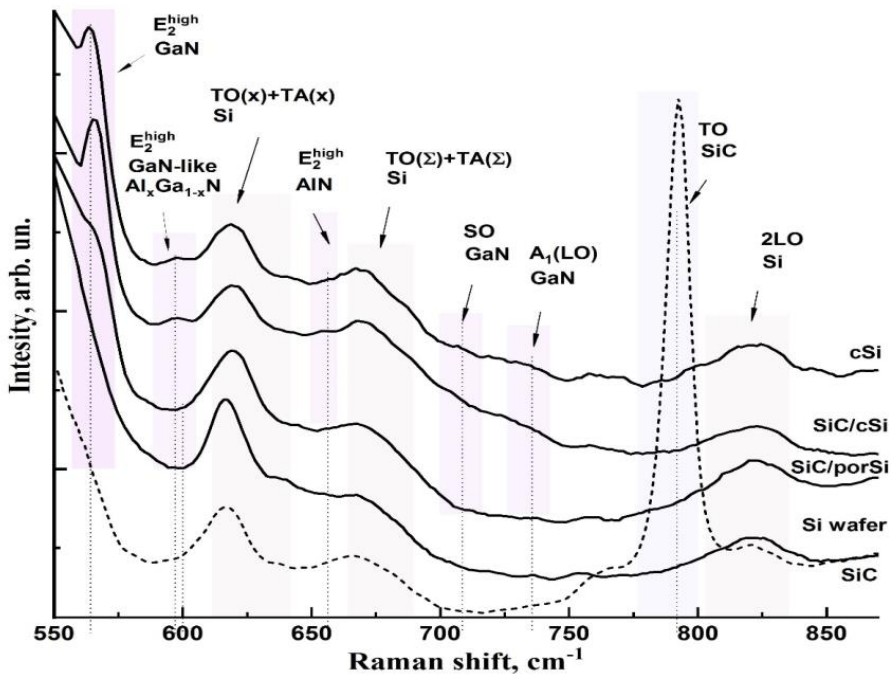

Figure 3. Region 530–900 cm^{-1} in the Raman spectra of the investigated heterostructures, silicon wafer, and SiC reference.

According to the Raman scattering tensor, single crystals GaN and AlN with a wurtzite crystal structure (space group P3m1) have a characteristic set of longitudinal optical (LO) and transverse optical (TO) phonon modes near the center of the Brillouin zone in their spectrum [31].

In our study, the Raman spectra were recorded in the z (xy) z^{-} geometry for the $Al_xGa_{1-x}N$/GaN nanoheterostructures. Considering the orientation of the sample and in accordance with the selection rule, the Raman spectra of GaN and $Al_xGa_{1-x}N$ contained characteristic maxima that can be correlated with the phonon modes A_1(TO), E_1(TO), and E_2^{high}, which are characteristic of GaN and $Al_xGa_{1-x}N$ crystals with a wurtzite structure [32].

The results of the Raman spectroscopy (see Figure 3) confirm the X-ray diffraction data regarding the wurtzite (hexagonal) structure of the layers of the investigated heterostructures, and are in good agreement with previously published works in which epitaxial GaN, AlN, and AlGaN films grown by different epitaxial methods (MOCVD, MBE, and CVD) were studied, for which the crystal plane [0001] of the epilayer was parallel to the [111] plane of the silicon substrate.

The most intense spectrum here is the Raman mode around 565–566 cm^{-1}, attributed to the E_2^{high} phonon and the oscillation near 730–735 cm^{-1}, which is the A1 (LO) mode of wurtzite GaN. The E_2^{high} and A1 (LO) phonon modes (labeled in Figure 3) represent the vibrations of the atoms in the ***c*** plane (parallel to the *a* axis) and along the *c* axis, respectively [33,34]. The feature in the spectrum around 653 cm^{-1} corresponds to the E_2^{high} AlN mode, the strongest of the resolved modes in the wurtzite AlN films for the *z (xy) z′* backscattering geometry used in our experiment [35].

Regarding the Raman response from the $Al_xGa_{1-x}N$ solid solution layer, and E_2^{high} GaN-like phonon mode localized at 595–600 cm^{-1} is present in the spectra of the three heterostructures. The position of this mode in the Raman spectra is determined not only by the composition of the solid solution [34] but also depends on the stresses arising in the thin epitaxial layer.

Another peculiarity in the spectra of cSi, SiC/sSi, and SiC/porSi heterostructures is the presence of a broad maximum in the spectra at 705 cm^{-1}. This oscillation, according to the authors of [36], can be attributed to the surface-active phonon mode of SO GaN.

In order to accurately determine the composition and frequencies of the low-intensity vibrations in the Raman spectra of cSi, SiC/CSi, and SiC/porSi samples, we performed a decomposition of the experimental Raman spectra into their various components. Simulations were performed using the Fytik software environment designed for spectral signal deconvolution, in particular Raman scattering. The Pearson 4-parameter function was chosen as the approximating function because its use provides a better approximation of the narrow bands in the Raman spectrum. The decomposition was performed so as to include the contribution from the low-intensity bands present in the spectrum. During the deconvolution step of the experimental spectra, we did not correct the baseline and did not remove the most intense mode, attributed to the TO mode of silicon from the spectrum, since this could introduce an error in determining the exact position of the modes of the vibrations belonging to the epitaxial layers.

The results of the decomposition are shown in Figure 4 and Table 1, showing the frequencies of the main vibrations attributed to GaN, AlN, and $Al_xGa_{1-x}N$ (marked in color in the spectra). It should be noted that a number of modes presented in the decomposition (indicated by the dotted line) that are not attributed to a particular structure are presumably related to the vibrations of silicon.

Table 1. Frequencies of the fundamental vibrations attributed to GaN, AlN, and $Al_xGa_{1-x}N$ from the Raman spectra decomposition results.

Sample	Frequencies of Fundamental Vibrations, cm^{-1}						Biaxial Stress in GaN, GPa
	GaN E_2^{high}	GaN-Like $Al_xGa_{1-x}N$	E_2^{high} AlN-Like	GaN SO	GaN A_1(LO)	SiC TO	
cSi	565.4	597.1	653.1	705.8	731.8	-	−0.456
SiC/cSi	565.2	596.2	652.7	707.4	733.2	794.0	−0.500
SiC/porSi	565.8	598.2	656.8	705.3	730.1	792.8	−0.370

It should be noted that deconvolution of the experimental spectra allowed us to isolate the vibrations occurring in the region of 792.8–794.0 cm^{-1}, which are not clearly observed in the spectrum but can be attributed to silicon carbide. According to the X-ray analysis results, the silicon carbide layer formed in two images (SiC/cSi and SiC/porSi) is a cubic 3C-SiC modification. It is known that only two modes, 796 and 972 cm^{-1}, are present in the Raman spectra of 3C-SiC [37]. They refer to the transverse optical (TO) and longitudinal optical (LO) phonons, respectively. A comparison of the data obtained (Table 1, Figures 3 and 4) for both the SiC reference sample and the SiC/cSi and porSi/SiC heterostructures confirms the cubic polymorphic type of silicon carbide formed in our structures, based on atomic substitution technology. The 1.2 cm^{-1} shift in the TO mode position of SiC observed in the SiC/cSi and porSi/SiC samples is due to the different structural imperfections of the silicon carbide. It is known that if the silicon carbide symmetry decreases from perfect cubic symmetry due to the formation of other polytypes or due to the introduction of random packing defects, degeneracy is lost and the TO phonon mode shifts to a lower wavenumber. As the number of defects increases, the observed signal widens and additional peaks with a lower wavenumber appear due to Raman scattering caused by packing disorder [38], as observed in the spectrum of the reference sample (see Figure 3).

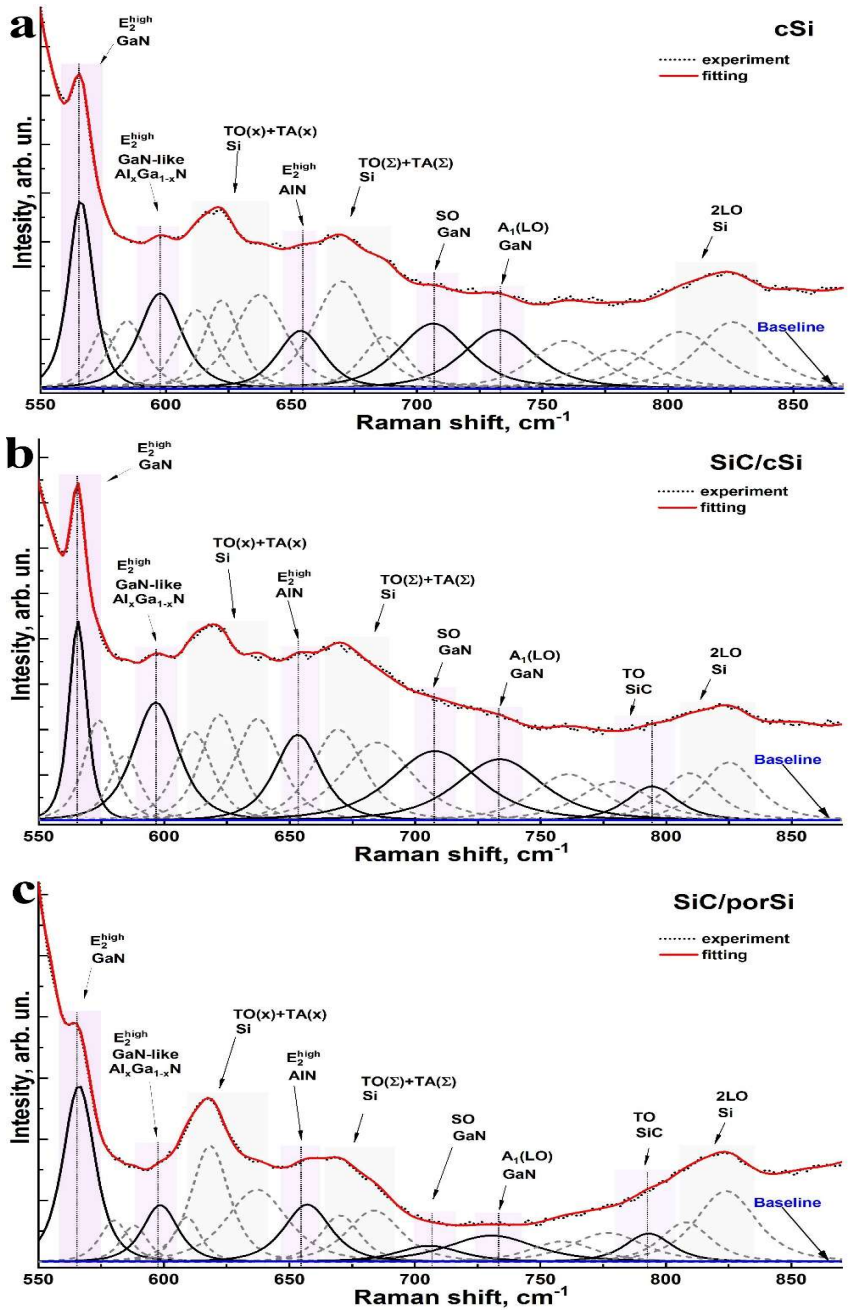

Figure 4. Results of the Raman spectra decomposition of heterostructures grown on cSi, SiC/cSi, and SiC/porSi substrates.

As for the GaN SO phonon, despite the fact that this oscillation is present in the spectra of all heterostructures, its intensity in the case of the SiC/porSi sample is much lower (see Figure 3). This is probably due to the surface morphology of the SiC/porSi sample, which is characterized by a lower coalescence of nanocolumns. Moreover, the frequency of the SO mode depends on the shape, size, and dielectric constant of the environment [36]. In our study, according to the atomic force microscopy data, the average size of the nanocolumns for the three samples lies in the region of 70–110 nm. According to the theoretical model [36], the SO phonon mode for GaN columns of an average diameter of 100 nm is expected to be about 705 cm^{-1}, which is close to what we observed experimentally, assuming that this mode has a predominantly E_1 symmetry.

It should be noted that the position of the E_2^{high} mode maxima for GaN and AlN in the Raman spectra of heterostructures differs from the frequencies of these modes that are

typical for unstressed pure bulk single crystals, which is a consequence of the appearance of deformation in the epitaxial layers of heterostructures due to the essential difference in parameters of the crystal lattice of these materials. Thus, the occurrence of tensile stresses in the epitaxial layer leads to a shift in the phonon mode to the low-frequency region of the spectrum with respect to the position of this maximum in the spectrum of completely non-tensioned material. Similarly, the shift of the phonon mode maximum to the high-frequency region corresponds to the appearance of compressive stresses in the epitaxial layer.

It is well known that in terms of linear approximation, the change in frequency (shift) of a particular phonon mode in the Raman spectrum of a particular material, under the influence of mechanical stresses that do not change the symmetry of the crystal, can be expressed as:

$$\Delta\omega = K_R \sigma_{xx} \tag{2}$$

where σ_{xx} is the biaxial stress value in the epitaxial layer, and K_R is the biaxial stress conversion factor, showing the degree of biaxial stress conversion to the Raman frequency shift.

Analysis of the current literature shows that the linear stress coefficient for the E_2^{high} mode of GaN takes a value of between 2.77 $\left(\mathrm{cm}^{-1}\cdot\mathrm{GPa}^{-1}\right)$ [39,40] and 4.3 $\left(\mathrm{cm}^{-1}\cdot\mathrm{GPa}^{-1}\right)$ [41], depending on the type of substrate [42]. However, as has been theoretically shown and experimentally confirmed [43,44], the conversion factor of the biaxial stress to the Raman frequency shift is significantly dependent on the crystal plane type of the substrate crystal, which is often neglected in calculations. In view of the above, in our calculations, we used a value of K_R = 4.596 $\left(\mathrm{cm}^{-1}\cdot\mathrm{GPa}^{-1}\right)$, which is typical of epitaxial film growth on the (111) Si plane [43,44]. In terms of the linear voltage coefficient K_R for the E_2^{high} mode of AlN, this value is 3.39 $\left(\mathrm{cm}^{-1}\cdot\mathrm{GPa}^{-1}\right)$ [35,42]. The characteristic value of the frequency position of the E_2^{high} mode for undeformed GaN is ~567.5 cm^{-1} [39,45], while for the E_2^{high} mode of undeformed AlN, it is ~657.4 cm^{-1} [35].

The value of biaxial stress in the GaN epitaxial layer, as calculated from Raman spectra, is presented in Table 1. The value of biaxial stress σ_{xx} in the AlN epitaxial layer, determined similarly from the E_2^{high} AlN mode shift, takes the values of −1.27, −1.39 and −0.18 GPa for the samples of cSi, SiC/cSi, and SiC/porSi, respectively. The detected downward trend of this value for AlN, depending on the type of substrate, correlates with that calculated for the GaN layer.

In terms of the $Al_xGa_{1-x}N$ solid solution, the phonon E_2^{high} GaN-like mode experiences a shift from its position characteristic of the $Al_xGa_{1-x}N$ solid solution. Thus, according to the literature data, the position of this lattice oscillation, depending on the composition of the $Al_xGa_{1-x}N$ solid solution for bulk [46] and thin films [34], can be estimated as:

$$\omega(Al_xGa_{1-x}N) = (567 \pm 1) + (40 \pm 3)x,\ \mathrm{cm}^{-1} \tag{3}$$

Thus, according to the authors of (18), for $Al_xGa_{1-x}N$ with x~0.60, a shift of ~10 cm^{-1} is observed with respect to the position of this vibration in the experimental spectrum. Assuming the validity of the elasticity theory and isotropy in the strain plane, the residual strain in the ε_{xx} plane and the axial strain ε_{zz} are related to the Raman shift value by a strain potential approximation, calculated as:

$$\Delta\omega = 2a\varepsilon_{xx} + b\varepsilon_{zz} \tag{4}$$

where a = 818.6 ± 14 cm^{-1} and b = 797 ± 60 cm^{-1}, which are the two phonon strain potential constants for the E_2^{high} GaN-like phonon mode, as reported in [47].

4. Conclusions

Since many of the properties of nitride-based epitaxial devices are determined by the substrate used to create them, the data set obtained in our work using the micro-Raman spectroscopy technique allowed us to establish the features of a typical transistor ultra-thin structure formation on hybrid substrates, incorporating silicon carbide and porous silicon layers, and to compare these features with the growth seen on standard cSi substrates.

Epitaxial GaN and $Al_xGa_{1-x}N$ epitaxial layers, in film grown by the proposed technology on cSi, SiC/cSi, and SiC/porSi substrates included in the thin film nanoheterostructure, have a wurtzite crystal structure, as confirmed by Raman spectroscopy data. At the same time, the SiC layer formed by atomic substitution has the symmetry of a cubic 3C-SiC polytype, while the use of a nanoporous silicon porSi sublayer, obtained by electrochemical etching, yields an oriented growth of silicon carbide on it.

Calculations of the biaxial strains in GaN and $Al_xGa_{1-x}N$ show that the lowest level of residual strain is observed in the GaN epilayers of a typical transistor with an ultra-thin structure, grown on a SiC/porSi hybrid substrate. Moreover, the GaN layer on the SiC/porSi hybrid substrate is characterized by an almost two-fold reduction of the residual stresses, in comparison with the growth seen on SiC/Si substrates.

Prior to our research, the success of technological approaches regarding the growth of nitrides on compliant substrates of porous silicon or silicon carbide has been repeatedly demonstrated. As noted above, the growth of gallium nitride layers on porous silicon has been achieved previously in a number of works, including our own. Nitride films were grown at various temperatures on porous silicon substrates via gas-phase epitaxy from organometallic compounds [48,49], molecular beam epitaxy [12,16], as well as using an RF magnetron sputtering system [50].

Additionally, a positive effect on the final properties of epitaxial nitride layers has been obtained by using SiC/Si and SiC/porSi/Si compliant substrates, which has also been noted in several other studies [16,51]. However, all the above-mentioned works refer to sufficiently bulky layers of gallium nitride, while in our current work, the growth of a thin-film nanoheterostructure is implemented on a hybrid SiC/porSi substrate.

Thus, a comparison of our experimental results and information from already published literature sources shows that the use of a hybrid compliant substrate containing a porous silicon interlayer and a silicon carbide layer has several undeniable advantages for the growth of ultra-thin AlGaN/GaN nanoheterostructures, without needing thick $A_{III}N$ buffer layers. Direct growth onto a hybrid compliant substrate SiC/porSi leads to the significant relaxation of elastic stresses between the silicon and silicon carbide and, consequently, to the much lower defectiveness of the silicon carbide layers, which is ultimately reflected in the structural quality and optical characteristics of $A_{III}N$ nitride-based ultra-thin transistor structures.

Author Contributions: Conceptualization, methodology, investigation A.L. and P.S.; visualization A.O.R.; writing and investigation D.G. and A.M. All authors have read and agreed to the published version of the manuscript.

Funding: This work was funded by grant no. 19-72-10007 from the Russian Science Foundation. The work of P.S. and A.M. was supported by the Ministry of Education and Science of the Russian Federation (grant No. FZGU-2020-0036 and No. FSRM-2020-0008). As a part of access to scientific equipment and methodology, this study was supported by the Ministry of Science and Higher Education of Russia under Agreement No. 075-15-2021-1351.

Institutional Review Board Statement: The study did not require ethical approval.

Informed Consent Statement: Not applicable.

Data Availability Statement: Not applicable.

Acknowledgments: The authors would like to thank Anatoly Lukin for their help with the experiments.

Conflicts of Interest: The authors declare no conflict of interest.

References

1. Liang, F.; Feng, M.; Huang, Y.; Sun, X.; Zhan, X.; Liu, J.; Sun, Q.; Wang, R.; Ge, X.; Ning, J.; et al. AlGaN-Based Schottky Barrier Deep Ultraviolet Photodetector Grown on Si Substrate. *Opt. Express* **2020**, *28*, 17188. [CrossRef] [PubMed]
2. Jang, W.-H.; Kim, H.-S.; Kang, M.-J.; Cho, C.-H.; Cha, H.-Y. Recessed AlGaN/GaN UV Phototransistor. *JSTS* **2019**, *19*, 184–189. [CrossRef]
3. Encomendero, J.; Faria, F.A.; Islam, S.M.; Protasenko, V.; Rouvimov, S.; Sensale-Rodriguez, B.; Fay, P.; Jena, D.; Xing, H.G. New Tunneling Features in Polar III-Nitride Resonant Tunneling Diodes. *Phys. Rev. X* **2017**, *7*, 041017. [CrossRef]
4. Zhou, Y.; Mi, M.; Yang, M.; Han, Y.; Wang, P.; Chen, Y.; Liu, J.; Gong, C.; Lu, Y.; Zhang, M.; et al. High Performance Millimeter-Wave InAlN/GaN HEMT for Low Voltage RF Applications via Regrown Ohmic Contact with Contact Ledge Structure. *Appl. Phys. Lett.* **2022**, *120*, 062104. [CrossRef]
5. Zheng, Y.; Cao, B.; Tang, X.; Wu, Q.; Wang, W.; Li, G. Vertical 1D/2D Heterojunction Architectures for Self-Powered Photodetection Application: GaN Nanorods Grown on Transition Metal Dichalcogenides. *ACS Nano* **2022**, *16*, 2798–2810. [CrossRef]
6. Zheng, Z.; Zhang, L.; Song, W.; Feng, S.; Xu, H.; Sun, J.; Yang, S.; Chen, T.; Wei, J.; Chen, K.J. Gallium Nitride-Based Complementary Logic Integrated Circuits. *Nat. Electron.* **2021**, *4*, 595–603. [CrossRef]
7. Gkanatsiou, A.; Lioutas, C.B.; Frangis, N.; Polychroniadis, E.K.; Prystawko, P.; Leszczynski, M. Electron Microscopy Characterization of AlGaN/GaN Heterostructures Grown on Si (111) Substrates. *Superlattices Microstruct.* **2017**, *103*, 376–385. [CrossRef]
8. Sugawara, Y.; Ishikawa, Y.; Watanabe, A.; Miyoshi, M.; Egawa, T. Observation of Reaction between a-Type Dislocations in GaN Layer Grown on 4-in. Si(111) Substrate with AlGaN/AlN Strained Layer Superlattice after Dislocation Propagation. *J. Cryst. Growth* **2017**, *468*, 536–540. [CrossRef]
9. Bessolov, V.N.; Karpov, D.V.; Konenkova, E.V.; Lipovskii, A.A.; Osipov, A.V.; Redkov, A.V.; Soshnikov, I.P.; Kukushkin, S.A. Pendeo-Epitaxy of Stress-Free AlN Layer on a Profiled SiC/Si Substrate. *Thin Solid Film.* **2016**, *606*, 74–79. [CrossRef]
10. Katagiri, M.; Fang, H.; Miyake, H.; Hiramatsu, K.; Oku, H.; Asamura, H.; Kawamura, K. MOVPE Growth of GaN on Si Substrate with 3C-SiC Buffer Layer. *Jpn. J. Appl. Phys.* **2014**, *53*, 05FL09. [CrossRef]
11. Kukushkin, S.A.; Mizerov, A.M.; Osipov, A.V.; Redkov, A.V.; Timoshnev, S.N. Plasma Assisted Molecular Beam Epitaxy of Thin GaN Films on Si(111) and SiC/Si(111) Substrates: Effect of SiC and Polarity Issues. *Thin Solid Film.* **2018**, *646*, 158–162. [CrossRef]
12. Seredin, P.V.; Goloshchapov, D.L.; Lenshin, A.S.; Mizerov, A.M.; Zolotukhin, D.S. Influence of Por-Si Sublayer on the Features of Heteroepitaxial Growth and Physical Properties of In x Ga 1-x N/Si(111) Heterostructures with Nanocolumn Morphology of Thin Film. *Phys. E Low-Dimens. Syst. Nanostructures* **2018**, *104*, 101–110. [CrossRef]
13. Seredin, P.V.; Lenshin, A.S.; Zolotukhin, D.S.; Arsentyev, I.N.; Zhabotinskiy, A.V.; Nikolaev, D.N. Impact of the Substrate Misorientation and Its Preliminary Etching on the Structural and Optical Properties of Integrated GaAs/Si MOCVD Heterostructures. *Phys. E Low-Dimens. Syst. Nanostructures* **2018**, *97*, 218–225. [CrossRef]
14. Seredin, P.V.; Lenshin, A.S.; Zolotukhin, D.S.; Arsentyev, I.N.; Nikolaev, D.N.; Zhabotinskiy, A.V. Experimental Study of Structural and Optical Properties of Integrated MOCVD GaAs/Si(001) Heterostructures. *Phys. B Condens. Matter* **2018**, *530*, 30–37. [CrossRef]
15. Seredin, P.V.; Lenshin, A.S.; Mizerov, A.M.; Leiste, H.; Rinke, M. Structural, Optical and Morphological Properties of Hybrid Heterostructures on the Basis of GaN Grown on Compliant Substrate Por-Si(111). *Appl. Surf. Sci.* **2019**, *476*, 1049–1060. [CrossRef]
16. Seredin, P.V.; Leiste, H.; Lenshin, A.S.; Mizerov, A.M. Effect of the Transition Porous Silicon Layer on the Properties of Hybrid GaN/SiC/Por-Si/Si(1 1 1) Heterostructures. *Appl. Surf. Sci.* **2020**, *508*, 145267. [CrossRef]
17. Mizerov, A.M.; Timoshnev, S.N.; Sobolev, M.S.; Nikitina, E.V.; Shubina, K.Y.; Berezovskaia, T.N.; Shtrom, I.V.; Bouravleuv, A.D. Features of the Initial Stage of GaN Growth on Si(111) Substrates by Nitrogen-Plasma-Assisted Molecular-Beam Epitaxy. *Semiconductors* **2018**, *52*, 1529–1533. [CrossRef]
18. Kukushkin, S.A.; Osipov, A.V. Theory and Practice of SiC Growth on Si and Its Applications to Wide-Gap Semiconductor Films. *J. Phys. D Appl. Phys.* **2014**, *47*, 313001. [CrossRef]
19. Lenshin, A.S.; Seredin, P.V.; Kashkarov, V.M.; Minakov, D.A. Origins of Photoluminescence Degradation in Porous Silicon under Irradiation and the Way of Its Elimination. *Mater. Sci. Semicond. Processing* **2017**, *64*, 71–76. [CrossRef]
20. Fernández-Garrido, S.; Koblmüller, G.; Calleja, E.; Speck, J.S. In Situ GaN Decomposition Analysis by Quadrupole Mass Spectrometry and Reflection High-Energy Electron Diffraction. *J. Appl. Phys.* **2008**, *104*, 033541. [CrossRef]
21. Ahmad, F.; Kumar, R.; Kushvaha, S.S.; Kumar, M.; Kumar, P. Charge Transfer Induced Symmetry Breaking in GaN/Bi2Se3 Topological Heterostructure Device. *NPJ 2D Mater. Appl.* **2022**, *6*, 12. [CrossRef]
22. Li, X.; Pongprueksa, P.; Van Landuyt, K.; Chen, Z.; Pedano, M.; Van Meerbeek, B.; De Munck, J. Correlative Micro-Raman/EPMA Analysis of the Hydraulic Calcium Silicate Cement Interface with Dentin. *Clin. Oral Investig.* **2016**, *20*, 1663–1673. [CrossRef] [PubMed]
23. Seredin, P.V.; Glotov, A.V.; Domashevskaya, E.P.; Arsentyev, I.N.; Vinokurov, D.A.; Tarasov, I.S.; Zhurbina, I.A. The Substructure and Luminescence of Low-Temperature AlGaAs/GaAs(100) Heterostructures. *Semiconductors* **2010**, *44*, 184–188. [CrossRef]
24. Seredin, P.V.; Glotov, A.V.; Ternovaya, V.E.; Domashevskaya, E.P.; Arsentyev, I.N.; Vinokurov, D.A.; Stankevich, A.L.; Tarasov, I.S. Effect of Silicon on Relaxation of the Crystal Lattice in MOCVD–Hydride AlxGa1−x As:Si/GaAs(100) Heterostructures. *Semiconductors* **2011**, *45*, 481–492. [CrossRef]
25. Spizzirri, P.G.; Fang, J.-H.; Rubanov, S.; Gauja, E.; Prawer, S. Nano-Raman Spectroscopy of Silicon Surfaces. *arXiv* **2010**, arXiv:1002.2692.

26. Iatsunskyi, I.; Jurga, S.; Smyntyna, V.; Pavlenko, M.; Myndrul, V.; Zaleska, A. Raman Spectroscopy of Nanostructured Silicon Fabricated by Metal-Assisted Chemical Etching. In Proceedings of the SPIE—The International Society for Optical Engineering, Brussels, Belgium, 1 May 2014; Volume 9132.
27. Seredin, P.V.; Goloshchapov, D.L.; Lenshin, A.S.; Kasatkin, I.A. Effect of Combination of Etching Modes on the Design, Structural and Optical Properties of the Compliant Substrates Based on Porous Silicon. *Opt. Mater.* **2021**, *119*, 111358. [CrossRef]
28. Wong, L.H.; Wong, C.C.; Liu, J.P.; Sohn, D.K.; Chan, L.; Hsia, L.C.; Zang, H.; Ni, Z.H.; Shen, Z.X. Determination of Raman Phonon Strain Shift Coefficient of Strained Silicon and Strained SiGe. *Jpn. J. Appl. Phys.* **2005**, *44*, 7922–7924. [CrossRef]
29. Dariani, R.S.; Ahmadi, Z. Study of Porous Silicon Structure by Raman Scattering. *Optik* **2013**, *124*, 5353–5356. [CrossRef]
30. Li, Q.; Qiu, W.; Tan, H.; Guo, J.; Kang, Y. Micro-Raman Spectroscopy Stress Measurement Method for Porous Silicon Film. *Opt. Lasers Eng.* **2010**, *48*, 1119–1125. [CrossRef]
31. Olivier, A.; Wang, H.; Koke, A.; Baillargeat, D. Gallium Nitride Nanowires Grown by Low Pressure Chemical Vapour Deposition on Silicon Substrate. *Int. J. Number Theory* **2014**, *11*, 243. [CrossRef]
32. Zeng, Y.; Ning, J.; Zhang, J.; Jia, Y.; Yan, C.; Wang, B.; Wang, D. Raman Analysis of E2 (High) and A1 (LO) Phonon to the Stress-Free GaN Grown on Sputtered AlN/Graphene Buffer Layer. *Appl. Sci.* **2020**, *10*, 8814. [CrossRef]
33. Davydov, V.Y.; Kitaev, Y.E.; Goncharuk, I.N.; Smirnov, A.N.; Graul, J.; Semchinova, O.; Uffmann, D.; Smirnov, M.B.; Mirgorodsky, A.P.; Evarestov, R.A. Phonon Dispersion and Raman Scattering in Hexagonal GaN and AlN. *Phys. Rev. B* **1998**, *58*, 12899–12907. [CrossRef]
34. Feng, Y.; Saravade, V.; Chung, T.-F.; Dong, Y.; Zhou, H.; Kucukgok, B.; Ferguson, I.T.; Lu, N. Strain-Stress Study of AlxGa1−xN/AlN Heterostructures on c-Plane Sapphire and Related Optical Properties. *Sci. Rep.* **2019**, *9*, 10172. [CrossRef] [PubMed]
35. Lughi, V.; Clarke, D.R. Defect and Stress Characterization of AlN Films by Raman Spectroscopy. *Appl. Phys. Lett.* **2006**, *89*, 241911. [CrossRef]
36. Pfüller, C.; Ramsteiner, M.; Brandt, O.; Grosse, F.; Rathsfeld, A.; Schmidt, G.; Geelhaar, L.; Riechert, H. Raman Spectroscopy as a Probe for the Coupling of Light into Ensembles of Sub-Wavelength-Sized Nanowires. *Appl. Phys. Lett.* **2012**, *101*, 083104. [CrossRef]
37. Okumura, H.; Sakuma, E.; Lee, J.H.; Mukaida, H.; Misawa, S.; Endo, K.; Yoshida, S. Raman Scattering of SiC: Application to the Identification of Heteroepitaxy of SiC Polytypes. *J. Appl. Phys.* **1987**, *61*, 1134–1136. [CrossRef]
38. López-Honorato, E.; Brigden, C.; Shatwell, R.A.; Zhang, H.; Farnan, I.; Xiao, P.; Guillermier, P.; Somers, J. Silicon Carbide Polytype Characterisation in Coated Fuel Particles by Raman Spectroscopy and 29Si Magic Angle Spinning NMR. *J. Nucl. Mater.* **2013**, *433*, 199–205. [CrossRef]
39. Choi, S.; Heller, E.; Dorsey, D.; Vetury, R.; Graham, S. Analysis of the Residual Stress Distribution in AlGaN/GaN High Electron Mobility Transistors. *J. Appl. Phys.* **2013**, *113*, 093510. [CrossRef]
40. Dai, Y.; Li, S.; Gao, H.; Wang, W.; Sun, Q.; Peng, Q.; Gui, C.; Qian, Z.; Liu, S. Stress Evolution in AlN and GaN Grown on Si(111): Experiments and Theoretical Modeling. *J. Mater. Sci. Mater. Electron.* **2016**, *27*, 2004–2013. [CrossRef]
41. Tripathy, S.; Chua, S.J.; Chen, P.; Miao, Z.L. Micro-Raman Investigation of Strain in GaN and AlxGa1−xN/GaN Heterostructures Grown on Si(111). *J. Appl. Phys.* **2002**, *92*, 3503–3510. [CrossRef]
42. Zhao, D.G.; Xu, S.J.; Xie, M.H.; Tong, S.Y.; Yang, H. Stress and Its Effect on Optical Properties of GaN Epilayers Grown on Si(111), 6H-SiC(0001), and c-Plane Sapphire. *Appl. Phys. Lett.* **2003**, *83*, 677–679. [CrossRef]
43. Qiu, W.; Ma, L.; Li, Q.; Xing, H.; Cheng, C.; Huang, G. A General Metrology of Stress on Crystalline Silicon with Random Crystal Plane by Using Micro-Raman Spectroscopy. *Acta Mech. Sin.* **2018**, *34*, 1095–1107. [CrossRef]
44. De Wolf, I. Relation between Raman Frequency and Triaxial Stress in Si for Surface and Cross-Sectional Experiments in Microelectronics Components. *J. Appl. Phys.* **2015**, *118*, 053101. [CrossRef]
45. Park, A.H.; Seo, T.H.; Chandramohan, S.; Lee, G.H.; Min, K.H.; Lee, S.; Kim, M.J.; Hwang, Y.G.; Suh, E.-K. Efficient Stress-Relaxation in InGaN/GaN Light-Emitting Diodes Using Carbon Nanotubes. *Nanoscale* **2015**, *7*, 15099–15105. [CrossRef] [PubMed]
46. Haboeck, U.; Siegle, H.; Hoffmann, A.; Thomsen, C. Lattice Dynamics in GaN and AlN Probed with First- and Second-Order Raman Spectroscopy. *Phys. Status Solidi (C)* **2003**, *0*, 1710–1731. [CrossRef]
47. Davydov, V.Y.; Averkiev, N.S.; Goncharuk, I.N.; Nelson, D.K.; Nikitina, I.P.; Polkovnikov, A.S.; Smirnov, A.N.; Jacobson, M.A.; Semchinova, O.K. Raman and Photoluminescence Studies of Biaxial Strain in GaN Epitaxial Layers Grown on 6H–SiC. *J. Appl. Phys.* **1997**, *82*, 5097–5102. [CrossRef]
48. Boufaden, T.; Chaaben, N.; Christophersen, M.; El Jani, B. GaN Growth on Porous Silicon by MOVPE. *Microelectron. J.* **2003**, *34*, 843–848. [CrossRef]
49. Ishikawa, H.; Shimanaka, K.; Azfar, B.M.; Amir, M.; Hara, Y.; Nakanishi, M. Improved MOCVD Growth of GaN on Si-on-Porous-Silicon Substrates. *Phys. Status Solidi (C)* **2010**, *7*, 2049–2051. [CrossRef]
50. Abud, S.H.; Selman, A.M.; Hassan, Z. Investigation of Structural and Optical Properties of GaN on Flat and Porous Silicon. *Superlattices Microstruct.* **2016**, *97*, 586–590. [CrossRef]
51. Cherkashin, N.A.; Sakharov, A.V.; Nikolaev, A.E.; Lundin, V.V.; Usov, S.O.; Ustinov, V.M.; Grashchenko, A.S.; Kukushkin, S.A.; Osipov, A.V.; Tsatsul'nikov, A.F. Peculiarities of Epitaxial Growth of III–N LED Heterostructures on SiC/Si Substrates. *Tech. Phys. Lett.* **2021**, *47*, 753–756. [CrossRef]